

Seasonal and inter-annual variability of lower stratospheric age of air spectra

F. Ploeger¹ and T. Birner²

¹Institute for Energy and Climate Research: Stratosphere (IEK-7), Forschungszentrum Jülich, Jülich, Germany.

²Department of Atmospheric Science, Colorado State University, Fort Collins, CO, USA.

Correspondence to: XXX

Abstract. Trace gas transport in the lower stratosphere is investigated by analysing seasonal and inter-annual variations of the age of air spectrum – the probability distribution of stratospheric transit times. Age spectra are obtained using the Lagrangian transport model CLaMS driven by ERA-Interim winds and total diabatic heating rates, and using a time-evolving boundary-impulse-response (BIER) method based on multiple tracer pulses. Seasonal age spectra show large deviations from an idealized stationary uni-modal shape. Multiple modes emerge in the spectrum throughout the stratosphere, strongest at high latitudes, caused by the interplay of seasonally varying tropical upward mass flux, stratospheric transport barriers and recirculation. Inter-annual variations in transport (e.g., QBO) cause significant modulations of the age spectrum shape. In fact, one particular QBO phase may determine the spectrum’s mode during the following 2-3 years. Interpretation of the age spectrum in terms of transport contributions due to the residual circulation and mixing is generally not straightforward. Advection by the residual circulation turns out to represent the dominant pathway in the deep tropics and in the winter hemisphere extratropics above 500K, controlling the modal age in these regions. In contrast, in the summer hemisphere, particularly in the lowermost stratosphere, mixing represents the most probable pathway controlling the modal age.

1 Introduction

The composition of the lower stratosphere includes radiatively active trace gases such as water vapour and ozone, which strongly affect the Earth’s radiation budget and surface temperatures (e.g., Riese et al., 2012; Solomon et al., 2010). The trace gas distribution in this region is strongly shaped by the global-scale Brewer-Dobson circulation, which may be separated into a residual mean meridional mass circulation and additional eddy mixing (e.g., Holton et al., 1995; Butchart, 2014). Both the residual circulation and mixing are largely driven by breaking Rossby waves and, to some extent, gravity waves (e.g., Haynes et al., 1991; Haynes and Shuckburgh, 2000).

A commonly used diagnostic to study transport in the lower stratosphere is the mean age of air, the average transit time of a stratospheric air parcel since entering the stratosphere. However, stratospheric air parcels are affected by various mixing processes along their pathways. Hence, an air parcel consists of a mixture of air with different transit times and is more fully characterized by a transit time distribution, commonly referred to as the *age spectrum* (e.g., Hall and Plumb, 1994; Waugh and Hall, 2002). Mean age of air (the first moment of the age spectrum) only provides a succinct description of stratospheric transport

for narrow and nearly symmetric age spectra. Generally, the effects of different transport processes (e.g., residual mean mass transport and mixing) cannot be distinguished with a single measure such as mean age and may lead to puzzling results (e.g., Waugh and Hall, 2002).

One such puzzling result concerns potential changes in stratospheric transport in a changing climate. Climate models indicate a strengthening residual circulation causing decreasing mean age during recent decades and into the future (e.g., Butchart et al., 2010), whereas observations indicate weakly increasing or statistically insignificant mean age trends, depending on the region and length of the data set (e.g., Engel et al., 2009; Stiller et al., 2012; Haenel et al., 2015). Recently, progress has been made to reconcile these apparently contradictory results. When dividing the Brewer-Dobson circulation into a shallow and a deep branch, evidence for a strengthening circulation is found for the shallow branch from both models (e.g., Garny et al., 2011) and in-situ observations (Bönisch et al., 2011; Ray et al., 2010; Ray et al., 2014). Reanalyses indicate a long-term strengthening of the residual circulation (Abalos et al., 2015), which causes decreasing mean age. However, strong decadal variations and, in particular, changes in eddy mixing have been found to mask these long-term residual circulation driven age changes (Ploeger et al., 2015a).

Consideration of the full age spectrum compared to just the mean age comes with the benefit of allowing one to separate the effects of different transport processes and may ultimately lead to an improved understanding of stratospheric transport and its long-term changes. Most existing studies on stratospheric age spectra are based on the assumption of stationary atmospheric flow and approximate the age spectrum by the Green's function for the diffusion process, an inverse Gaussian distribution (e.g., Andrews et al., 2001; Schoeberl et al., 2005; Bönisch et al., 2009). Such an approximation is based on the fact that for tracers of long enough chemical lifetimes stationary stratospheric transport reduces to a 1D flux-gradient relationship (Plumb and Ko, 1992). The 1D diffusion Green's function has been used in the pioneering work of Hall and Plumb (1994) to illustrate the main characteristics of stratospheric age spectra. These studies lead to insights into a number of characteristics of stratospheric transport, including the relationship between mean age and the age spectrum. Consideration of the age spectrum has furthermore aided model intercomparisons of stratospheric transport (Hall, 1999). However, assuming stationary flow is a strong simplification as stratospheric transport shows variations on multiple time scales (e.g., seasonal, inter-annual) and is clearly non-stationary (e.g., Haine et al., 2008).

A few recent studies calculated time-dependent age spectra for non-stationary flow from Lagrangian back trajectories (Reithmeier et al., 2007; Diallo et al., 2012). All of these above mentioned studies based on back trajectories, however, did not incorporate the effects of small-scale mixing on transport (i.e., mixing of air masses between trajectories). The only published analyses, to our knowledge, of non-stationary age spectra for complete 3D transport (including mixing) are Li et al. (2012a), focussing on seasonality, and Li et al. (2012b), focussing on long-term trends. These studies found significant differences of seasonal age spectra from the idealized stationary shape, with the age spectrum within particular regions even showing multiple peaks (modes). However, their explanations for these seasonal variations and the multiple peaks are different, involving seasonality in tropical upward mass flux, the strength of the polar vortex transport barrier, or the existence of different circulation branches. A common understanding of the intricate age spectrum characteristics appears to be lacking. Moreover, regarding inter-annual age spectrum variations the only published results (Li et al., 2012a), to our knowledge, are based on a

model simulation without a quasi-biennial oscillation (QBO). Hence, age spectrum modulations by the QBO have not been studied in detail hitherto, although an indication of such modulation is contained in Ray et al. (2014, their Fig. 4).

Figure 1 illustrates several of the above mentioned age spectrum characteristics, highlighting additional insights that can be gained from consideration of the full age spectrum. The figure presents climatological wintertime age spectra along a given mean age contour of 2.5 years, calculated with the CLaMS model as described in Sect. 2. In general, stratospheric age spectra are characterized by skewed distributions with a long tail at old ages. As age spectra here are calculated for time-dependent flow, without any stationarity assumptions, these spectra show clear multi-modal shapes, with a strong regional dependence (as discussed in Sect. 3 and Sect. 6). Clearly, the spectrum shape significantly varies for the same mean, with a narrow spectrum at low latitudes and substantially broader spectra at higher latitudes. Quantifying the amount of young air and its variability and changes is important for understanding the transport of short-lived chemical species and pollution into the stratosphere (e.g., Schoeberl et al., 2005). This information requires evaluation of the full age spectrum and cannot be estimated from the mean age alone (e.g., Waugh and Hall, 2002).

The modal age, defined as the transit time of the age spectrum peak, by definition corresponds to the most probable transit time. The occurrence of multiple peaks (potentially of similar size) in time-varying age spectra indicates the challenging nature of interpreting the modal age correctly. Within the tropics, modal age is known to be closely related to the residual mean mass circulation (e.g., Waugh and Hall, 2002; Li et al., 2012b). In other regions of the stratosphere, where mixing processes have a predominant effect on transport (e.g., in the NH lower stratosphere during summer, see Konopka et al., 2015), this relation is expected to break down. However, no global analysis exists to our knowledge which systematically investigates the relationship between modal age, residual circulation strength, and mixing.

In this paper, we present a method to calculate stratospheric age spectra in the Chemical Lagrangian Model of the Stratosphere (CLaMS), a state-of-the-art reanalysis-driven chemistry transport model. This method is a further development of the approach by Li et al. (2012a), based on boundary impulse responses using multiple tracer pulses launched at the Earth's surface in the deep tropics, and allows one to calculate the age spectrum in a transient simulation without additional assumptions such as the smallness of inter-annual variability. The analyses focus on the following questions: (i) How large is the variability of lower stratospheric age spectra on seasonal to inter-annual time scales and how do multiple spectral peaks (modes) develop? (ii) How do residual circulation and mixing affect the age spectrum globally?

We describe our methodology in Sect. 2 and consider seasonal age spectrum variations in Sect. 3. The effects of residual circulation transport and mixing are investigated in Sect. 4. Inter-annual variability is discussed in Sect. 5. A discussion of the development of multiple modes in the spectrum is presented in Sect. 6. The final section concludes the paper.

2 Methodology

2.1 The CLaMS model simulation

The model used in this study is the Chemical Lagrangian model of the Stratosphere (CLaMS). CLaMS is a Lagrangian transport model with trace gas transport based on the motion of three-dimensional forward trajectories and an additional parametrization

of small-scale atmospheric mixing (e.g., McKenna et al., 2002; Konopka et al., 2004). This mixing parametrization induces strong mixing in regions of large flow deformations. Vertical transport in CLaMS is based on a hybrid σ - θ coordinate, which transforms smoothly from an orography-following coordinate ($\sigma = p/p_s$, with p pressure and p_s surface pressure) near the surface into potential temperature θ (see also Mahowald et al., 2002). Above $\sigma = 0.3$, hence throughout the stratosphere and the TTL, the hybrid vertical coordinate exactly equals potential temperature and the vertical velocity is determined by the total diabatic heating rate. Further details about this particular model set-up are described in Pommrich et al. (2014).

For this study, we carried out a simulation for the 1979–2013 period, with model transport driven by European Centre for Medium-Range Weather Forecasts (ECMWF) interim Reanalysis (ERA-Interim) winds (e.g., Dee et al., 2011). Furthermore, we implemented a method to calculate the age of air spectrum within the model, which will be described in detail next.

2.2 Age spectrum calculation

The solution to the continuity equation for a conserved and passive tracer with mixing ratio χ at location r and time t may be expressed as (e.g., Waugh and Hall, 2002):

$$\chi(r, t) = \int_0^{\infty} d\tau \chi(\Omega, t - \tau) G(r, t | \Omega, t - \tau). \quad (1)$$

The kernel $G(r, t | \Omega, t - \tau)$ is called the *boundary propagator*. This propagator is related to the transport operator's Green's function (see Holzer and Hall, 2000), and relates the tracer mixing ratio at (r, t) to the mixing ratio in the boundary source region Ω (chosen to be the tropical boundary layer, in the following) a time $\tau = t - t'$ ago. Here, t is called the *field time* when the tracer mixing ratio is sampled, whereas t' is called the *source time* when the tracer had last contact with Ω . Interpreting Eq. (1), $G(r, t | \Omega, t - \tau) d\tau$ is the mass fraction of air at (r, t) that had last been in contact with Ω between τ and $\tau + d\tau$ ago. For this reason, $G(r, t | \Omega, t - \tau)$ is a transit time distribution and has been termed the *age spectrum* by Hall and Plumb (1994). Note that the propagator G can be interpreted as a joint air mass origin and transit time distribution, such that integration over τ yields the mass fraction of air originating from Ω (e.g., Orbe et al., 2013).

For an inert tracer with a pulse in Ω at source time $t' = t'_0$ the source time history is given by $\chi(\Omega, t') = \delta(t' - t'_0)$, and Eq. (1) reduces to (recalling $t' = t - \tau$)

$$\chi(r, \tau + t'_0) = G(r, \tau + t'_0 | \Omega, t'_0). \quad (2)$$

Here, $G(r, \tau + t'_0 | \Omega, t'_0)$ is the *boundary impulse response* (BIR), the time-evolving response at location r to a δ -distribution boundary condition in Ω at time t'_0 . In general, as a function of transit time τ the BIR is not equal to the age spectrum, because the τ -dependency occurs in different arguments of G . Only for stationary flow the boundary propagator is time translation invariant and depends only on the transit time τ , such that the age spectrum and BIR are equal (e.g., Haine et al., 2008).

Equation (2) provides a method to calculate the boundary propagator G by using N different pulse tracers χ_i ($i = 1, \dots, N$), with pulses in Ω at times t'_i (e.g., Haine et al., 2008). The age spectrum, as a function of τ , may be constructed from these N pulse tracers at each field time t and location r as

$$G(r, t | \Omega, t - \tau_i) = \chi_i(r, t). \quad (3)$$

Hence, from N pulse tracers N pieces of information on the age spectrum at the discrete transit times $\tau_i = t - t'_i$ may be deduced. Recently, this BIR-method was used to investigate the seasonality (Li et al., 2012a) and long-term behaviour (Li et al., 2012b) of stratospheric age spectra in the Goddard Earth Observing System Chemistry-Climate Model (GEOSCCM).

Here, we use a total of $N = 60$ different boundary pulse tracers, with pulses released in the lowest model layer (orography following) in the tropics between 15°S – 15°N , constituting the source region Ω . This source region has been chosen similar to that of Li et al. (2012a) for ease of comparison. Variations of the source region (e.g., 10°S – 10°N , entire global surface layer) lead to qualitatively the same results. Note that another common choice, particularly for observationally based age spectrum estimates, is to define Ω as the tropical tropopause. Related differences for transit times are expected to be a few weeks to months, which is the time scale for transport from the surface to the tropopause. For each pulse, the particular tracer mixing ratio is set to unity in Ω for 30 days, and is set to zero in Ω otherwise. Pulses are launched every other month. Consequently, for the considered period 1979–2013 the first tracer pulse has source times in January 1979, the second tracer pulse in March 1979, and so on.

Figure 2 shows the evolution of the tracer mixing ratio in the meridional plane during the months following the pulse release. The dispersal of the tracer plume illustrates the known features of the global scale stratospheric Brewer-Dobson circulation. During the first months after release, the tracer-tagged air disperses throughout the troposphere and slowly ascends across the tropical tropopause into the stratosphere, with this tropical upwelling being stronger in NH winter than summer. Above the tropopause, the air is mixed rapidly (to high latitudes), with this mixing being stronger in the summer hemisphere (particularly for NH summer). In the winter hemisphere, meridional mixing to high latitudes is suppressed due to the existence of the polar vortex transport barrier. One year after release, the tracer has largely been washed out in the extratropical lower stratosphere via downward transport into the troposphere. In the tropics, on the other hand, the pulse air further ascends slowly within the tropical pipe (above about 450 K), well isolated from further mixing with the extratropics. For air masses leaving the surface during winter, a substantially higher fraction reaches the stratosphere compared to air released in summer (see two right columns in Fig. 2). In particular, after 3 years almost twice as much winter surface air is found in the stratosphere compared to summer surface air. We will further discuss this seasonal difference in Sect. 6.

The age spectrum calculation method in the transport model CLaMS is further illustrated in Fig. 3, which shows the BIR map at 400 K and 60°N , i.e. the propagator G versus field time and source time. Following the initial pulse at source time t' , each pulse tracer mixing ratio evolves with field time t producing a vertical section in the BIR map. The set of all tracers comprises the BIR map. Therefore, a vertical cut through the BIR map provides the boundary impulse response at a given source time t' as a function of field time t (e.g., the vertical dashed arrow shows the BIR for January 1995). A horizontal cut through the BIR map provides the age spectrum at a given field time as a function of source time, or equivalently of transit time by noting that $\tau = t - t'$ (e.g., the horizontal arrow shows the age spectrum for June 2002).

Due to the finite number of tracers used here ($N = 60$) initialized every other month in source time (i.e., 6 pulses per year for 10 years), the calculated age spectrum is truncated to a maximum transit time of ten years. We used results of a ten year long perpetual simulation (repeating 1979 winds) as initialization for the transient simulation starting at 1 January 1979. Therefore, values in the BIR map at source times before 1 January 1979 (and field times before 1989) will be influenced by this

initialization procedure. For this reason, we do not consider age spectra before 1989 in this paper, and calculate climatologies for the 1989–2013 period. Once all sixty tracers have been used (after the first ten years) the first tracer is reset to zero and then used for the pulse at source time January 1989, and so on for consecutive pulses. Hence, we obtain time-dependent age spectra at every day of the transient 1979–2013 simulation, with a resolution along the transit time axis of 2 months. Li et al. (2012a) showed that a 2-month resolution of the pulses is suitable for resolving the seasonal age spectrum variations, and it is therefore sufficient for the results presented in this paper.

Our implementation of the age spectrum method in CLaMS differs from the BIR calculation by Li et al. (2012a) and Li et al. (2012b), who considered time slice simulations and used each tracer only once. To emphasize the fact that the modified BIR tracer setting in CLaMS evolves with time in a transient simulation, we denote the age spectrum calculation as implemented here the *Boundary Impulse Evolving Response* (BIER) approach.

Figure 3b shows the annual mean age spectrum at 400 K in NH mid-latitudes at 60°N, the horizontal cut through the BIR map in Fig. 3a. The maximum of the spectrum (*modal age*, here highlighted as vertical black dashed line) corresponds to the most probable transit time and likely to the most probable pathway (to be discussed further below). The *mean age* (vertical black solid line) is defined as the first moment of the age spectrum

$$\Gamma(r, t) = \int_0^{\infty} d\tau \tau G(r, t | \Omega, t - \tau) \quad (4)$$

and strongly depends on the tail of the distribution. Another quantity characterizing the distribution is the age spectrum width

$$\Delta(r, t) = \sqrt{\frac{1}{2} \int_0^{\infty} d\tau [\tau - \Gamma(r, t)]^2 G(r, t | \Omega, t - \tau)}. \quad (5)$$

In addition, the red dashed line shows the residual circulation transit time (RCTT), the hypothetical transit time of an air parcel if it was advected by the residual circulation only (e.g., Rosenlof, 1995; Birner and Bönisch, 2011). RCTT's and their relation to mean age of air have recently been discussed by Garny et al. (2014). Here, RCTT's are calculated from 2D CLaMS backward trajectories in the latitude-potential temperature plane, driven by the ERA-Interim residual circulation in isentropic coordinates (\bar{v}^*, \bar{Q}^*), as described by Ploeger et al. (2015b). In this isentropic zonal mean formulation $\bar{v}^* = (\overline{\sigma v})/\bar{\sigma}$ and $\bar{Q}^* = (\overline{\sigma Q})/\bar{\sigma}$ are the mass-weighted zonal mean meridional and vertical velocities, where $\hat{\theta} = Q$ is the cross-isentropic vertical velocity and $\sigma = -g^{-1} \partial_{\theta} p$ is the density in isentropic coordinates, with p pressure and g the acceleration due to gravity (e.g., Andrews et al., 1987, Chapter 9). The RCTTs are calculated with respect to the 340 K surface. This causes a weak young bias of the RCTTs compared to age of air, corresponding to the transit time from the Earth's surface to 340 K. The relation between the age spectrum and the RCTT will be studied in Sect. 4.

A limitation of the described approach to calculate the age spectrum originates from the limited number of pulse tracers in the model, such that only the first ten years of the spectrum are calculated explicitly here. Because the mean of the distribution strongly depends on the spectrum's tail this leads to an underestimation of mean age. However, for transit times above about 4-5 years age spectra are generally found to decay roughly exponentially (cf. Fig. 3c). The corresponding decay rate is related to the exponential decay of the mixing ratio of a conserved tracer in the stratosphere (e.g., Ehhalt et al., 2004). To estimate the

age spectrum's tail for transit times larger than ten years, the spectrum may therefore be extrapolated using an exponential fit based on the values at transit times between 5-10 years (red dashed line in Fig. 3c), as explained in detail in Appendix A. A similar tail correction procedure was applied by Diallo et al. (2012). Throughout this paper we present the tail-corrected mean age.

5 Global mean age distributions for NH winter (DJF) and summer (JJA), as obtained from age spectra, are shown in Fig. 4, confirming well-known characteristics of the stratospheric Brewer-Dobson circulation. A stronger circulation during NH winter causes younger ages in the tropics, compared to the boreal summer season. Mean age is older in the winter than in the summer extratropics, due to stronger Brewer-Dobson circulation downwelling in the winter hemisphere and weaker transport barriers in the summer hemisphere. Particularly young mean age is found in the NH lower stratosphere during summer as a
 10 result of strong quasi-horizontal mixing during this season (Konopka et al., 2015). The effect of the correction for the finite spectrum tail is an increase of mean age of about half a year compared to the uncorrected ages, mainly at high altitudes and latitudes (see Appendix A for details). Comparison to mean age calculated from a model 'clock-tracer', an inert tracer with a linear increase in the boundary layer (see also Hall and Plumb, 1994), shows good agreement with the spectrum-based mean age and therefore affirms the internal consistency of the age spectrum calculation in the model (see Fig. 4 c/d).

15 3 Seasonality of age spectra

The climatological annual mean age spectrum in the NH lower stratosphere (here 400 K, 60°N) from the CLaMS simulation (black line in Fig. 5) is characterized by a skewed distribution with a maximum around half a year. This annual mean distribution is well approximated by the idealized age spectrum for stationary flow, as represented by an inverse Gaussian distribution, the Green's function for 1D diffusion (grey shading). For long-lived tracers stratospheric transport may be approximated by
 20 a one-dimensional flux-gradient relationship (Plumb and Ko, 1992). Motivated by this fact, Hall and Plumb (1994) discussed properties of the age spectrum by considering the Green's function for a one-dimensional diffusion process. Such a consideration requires the assumption of stationary flow (see Holzer and Hall, 2000, for a more general discussion). The 1D diffusion Green's function can be expressed in terms of the mean age and spectrum width as (e.g., Waugh and Hall, 2002, Eq. 9)

$$G^{\text{diff}}(\tau) = \sqrt{\frac{\Gamma^3}{4\pi\Delta^2\tau^3}} \cdot \exp\left(-\frac{\Gamma(t-\Gamma)^2}{4\Delta^2t}\right) \quad (6)$$

25 and is frequently used to approximate the age spectrum shape for deducing age of air information from observed tracers (e.g., Schoeberl et al., 2005).

The seasonal age spectra, however, show a more complicated structure with multiple peaks along the transit time axis (coloured lines in Fig. 5). The occurrence of multiple peaks in seasonal age spectra has already been noted and discussed in recent papers (e.g., Reithmeier et al., 2007; Diallo et al., 2012; Li et al., 2012a). Here, we simply present the CLaMS based
 30 findings and relate to published results in Sect. 6. In Fig. 5 the modal age, as determined by the apex of the largest peak in the seasonal age distribution, coincides with the youngest peak during spring, summer and fall and with the second peak during winter. Furthermore, the location of the mode strongly depends on the region (e.g., Sect. 4).

The occurrence of multiple peaks in the seasonal age spectrum (Fig. 5) reflects the seasonality of transport. The highest fraction of young air in the NH lower stratosphere at 400 K is found in NH summer (red line in Fig. 5). The BIR map in Fig. 3a shows that these air masses had left the boundary layer about half a year earlier, in the previous winter (source time of the peak corresponds to NH winter). Figure 5 further shows how the summertime peak of young air (transit times of about half a year) ages throughout the course of the year. The coloured crosses in the figure illustrate the position of the peak during the following seasons: at about 0.75 years during the following fall, ~ 1 year during the following winter, ~ 1.25 years during the following spring, with a ~ 1 -year offset from the original summer peak during the following year's summer, and so on. The evolution of the age spectrum peaks becomes even clearer in a presentation versus season and transit time in Fig. 6. An exceptionally high fraction of young air arrives in the extratropical NH lower stratosphere during spring and summer, causing the strong summertime peak at young transit times. This peak propagates to older transit times during the following months, and occurs around transit times of one year during next winter. A more detailed discussion of the processes affecting the age spectrum peaks will be presented in Sect. 6.

Consideration of the full age spectrum allows one to quantify air mass fractions corresponding to certain transit times. Of particular importance for short-lived chemical species in the lower stratosphere is the fraction of very young air with transit times below some threshold τ^* (denoted *fresh-air-fraction* F_{τ^*} in the following), which can be deduced from the age spectrum by integration over transit time

$$F_{\tau^*}(r, t) = \int_0^{\tau^*} d\tau G(r, t | \Omega, t - \tau). \quad (7)$$

This fresh-air-fraction is an important quantity for understanding the abundances of short-lived trace constituents, and we will discuss its seasonal variability in the following.

Figure 7a–b shows the fresh-air-fraction with transit times younger than six months (F_6) for NH winter and summer. In the tropical lower stratosphere, the F_6 is larger in NH winter than summer, consistent with the seasonality in tropical upwelling which maximizes in NH winter (e.g., Rosenlof, 1995). Although the strongest upwelling is displaced into the respective summer hemisphere (e.g., Seviour et al., 2011; Abalos et al., 2015), the corresponding F_6 in this region is lower than in the winter hemisphere tropics and subtropics (Fig. 7a–b). This indicates a significant impact of in-mixing of old air masses from the extratropics on the tropical composition, maximum during NH summer. Such mixing increases the amount of old air at low latitudes, consistent with an enhanced mass fraction of air older than two years in this region (Fig. 7c–d).

The two hemispheres show opposite annual cycles in F_6 , with the largest extratropical F_6 values in the lower stratosphere found during summer in each hemisphere. A striking hemispheric asymmetry exists in the fresh air fraction below about 450 K (Fig. 7a–b). In particular the NH lowest stratosphere is flushed with young air during summer (e.g., Hegglin and Shepherd, 2007; Bönisch et al., 2009), increasing F_6 there to about 20%. This flushing with young air has implications for the chemical composition of this region, for instance by enhancing the amount of short-lived species and pollutants. At levels closer to the extratropical tropopause the maximum in NH F_6 appears lagged by 1-2 months compared to the levels above (not shown). The timing of maximum youngest air in the extratropics during hemispheric summer to fall is consistent with strongest horizontal

transport from the tropics during each hemisphere's summer. Furthermore, the minimum tropical F_6 during NH summer is consistent with stronger horizontal eddy mixing in the NH than in the SH (e.g., Konopka et al., 2015).

Geographical distributions of F_6 and mean age at 400 K are shown for winter and summer in Fig. 8. Clearly, the largest F_6 values occur during NH winter directly above the tropopause over the Western Pacific, the Indian Ocean, and Central Africa.

5 During NH summer, the largest F_6 occur in a narrow band south of the equator and within the Asian monsoon anticyclone (from the Tibetan plateau and North India to the Middle East). The enhanced young air mass fractions in the Asian monsoon likely have implications for pollution transport into the lower stratosphere (see also Randel et al., 2010), as the Asian monsoon system is close to the geographical source regions of highest anthropogenic pollution in India and China. Both the fresh air fraction and mean age show a clear planetary wave signature at middle and high latitudes during NH winter.

10 The additional information included in the spectrum as compared to mean age is illustrated by comparing mean age with the fractions of either young or old air masses. The difference between mean age and F_6 increases with altitude and latitude (Fig. 7a–b). As mean age is strongly affected by the age spectrum's tail, for broader age spectra at higher altitudes and latitudes its structure more closely resembles that of the fraction of old air with transit time larger than two years (Fig. 7c–d). Especially the Southern polar vortex during June–August shows very old mean age and an almost vanishing fresh air fraction F_6 (Fig. 7b/d).

15 The large-scale geographical patterns of F_6 at 400 K largely resembles the geographical variability of the mean age distributions (Fig. 8c–d). On smaller spatial scales, however, the young air fraction and mean age patterns may differ significantly (e.g., compare the tongue of old air south of the Asian monsoon anticyclone in Fig. 8d in both diagnostics).

4 Residual circulation and mixing effects on age spectra

From a conceptual point of view, zonal mean stratospheric transport may be separated into net mass transport (given by the residual mean meridional circulation) and additional two-way mixing due to eddies (e.g., Andrews et al., 1987, chapter 9). The transit time corresponding to the residual circulation, the RCTT (see Sect. 2), describes the pure effect of residual circulation transport (e.g., Birner and Bönisch, 2011). Therefore, the difference between the RCTT and the “real” atmospheric transport time scale (the age of air) provides a measure of the effect of eddy mixing (Garny et al., 2014). The peak of the age spectrum (modal age) is related to the most probable transport time scale, likely corresponding to the most probable transport pathway.

25 Comparison between the modal age and the RCTT therefore allows an analysis of the regions and seasons where either the residual circulation or eddy mixing dominates stratospheric transport.

Figure 9 presents the age spectra at 400 K and 600 K for all latitudes during winter and summer, together with the corresponding modal ages, mean ages, and RCTTs. In the tropics, the age spectrum generally shows one distinct peak, hence a well-defined modal age, at time scales close to the RCTT. From the subtropics to high latitudes, however, the spectrum shape is characterized by multiple peaks of similar strength, and therefore the modal age is ill-defined. The annual cycle in tropical upwelling, with faster upwelling in NH winter compared to summer, is reflected in a younger tropical spectrum peak during winter (the 20°N/S average modal age is 3.5 months during NH winter versus 4.1 months during summer). The small difference

between the modal age and the RCTT in the lower tropical stratosphere at 400 K, with the modal age slightly older, shows an effect of in-mixing of old extratropical air into the tropics just above the tropopause.

At 600 K there is a clear separation of youngest air (around 1 year) in the tropics during both seasons, consistent with a tropical pipe model of stratospheric transport (Plumb, 1996). Interestingly, the modal age during NH summer appears at
5 somewhat older transit times, suggesting that recirculation of older air from the extratropics plays a more important role during this season than during NH winter.

At lower levels (here 400 K), steep latitudinal gradients in the fraction of youngest air (F_6) exist in mid-latitudes only during winter. These latitudinal gradients are significantly weaker during summer, in particular in the NH lower stratosphere where the high fraction of young air at high latitudes indicates strong horizontal transport from the tropics. This is consistent with
10 studies showing that the isolation of tropical air imposed by the subtropical transport barriers does not extend down to 400 K (e.g., Volk et al., 1996). The large difference between modal age and RCTT in the lower extratropical stratosphere (particularly poleward of about 50°N during NH summer) further indicates that transport in this region is predominantly related to mixing. On the other hand, equatorward of about 50°N modal age and RCTT agree well at both levels and seasons, which points to a more dominant role of residual circulation transport. Therefore, the age spectrum analysis is consistent with recently
15 published results relating the summertime “flushing” of the NH extratropics with young air to the combined effect of residual circulation transport equatorward of about 50°N , and quasi-horizontal mixing poleward of about 50°N (Bönisch et al., 2009; Konopka et al., 2015). In general, the existence of multiple spectral peaks in the extratropics questions the value of modal age as an reliable descriptor for age of air.

Profiles of modal age and RCTT at different latitude bands for winter and summer are compared in Fig. 10. Throughout the
20 tropics, the modal age agrees well with the RCTT and consequently transport is largely related to the residual circulation. The figure also includes a simple proxy for the time scale of tropical upward transport (only panels a and d) based on the definition of cross-isentropic vertical velocity $\dot{\theta} = \Delta\theta/\Delta t$. Note that this simple proxy significantly differs from both the modal age and the RCTT during NH summer above about 650 K. This is related to seasonal changes in the structure of tropical upwelling and apparently emerges at transit times longer than about 1.5 years. The wintertime high-latitude stratosphere above about
25 500 K ($55\text{--}85^\circ\text{N}$ during DJF, and $85\text{--}55^\circ\text{S}$ during JJA) represents another case where modal age and RCTT closely match and transport appears to be well described by the residual circulation. For all other regions and seasons modal age and RCTT differ, at least partly, and eddy mixing has a significant effect on stratospheric transport. The clearest difference between modal age and RCTT and therefore the strongest mixing effect emerges in the high-latitude ($55\text{--}85^\circ\text{N/S}$) lower stratosphere below about 500 K, in particular during summertime. However, apart from this exception the RCTT represents a good approximation to
30 modal age, but not mean age.

The comparison between modal age and RCTT is summarized in Fig. 11, which shows the percentage difference between RCTT and modal age $(\text{RCTT} - \text{mode})/\text{RCTT}$ for winter and summer. Small differences indicate a strong effect of the residual circulation on transport, as found throughout the deep tropics and in the respective winter hemisphere. The dipole pattern in each hemisphere below about 500 K, with RCTT smaller than the modal age in the tropics and larger than the modal age
35 poleward of about 50° , is related to the strong effect of eddy mixing at these levels. As eddies mix air quasi-horizontally

between the tropics and the extratropics, relatively old air is transported into the tropics while young air is transported into the extratropics. Therefore, in the tropics mixing causes an older modal age as compared to the pure residual circulation effect, reflected in the negative values in that region (Fig. 11). In the extratropics, mixing causes the modal age to be younger than resulting from pure residual circulation advection, and hence positive differences.

5 5 Inter-annual variability of the age spectrum related to the Quasi-Biennial Oscillation (QBO)

The Quasi-Biennial Oscillation QBO (e.g., Baldwin et al., 2001) represents the dominant mode of inter-annual variability in the tropical lower stratosphere. The GCMs used in recent studies (e.g., Reithmeier et al., 2007; Li et al., 2012a, b) did not include a QBO. Existing trajectory calculations based on reanalysis data (e.g., Diallo et al., 2012; Ray et al., 2014), while in principle including the QBO, have not analysed such effects in detail. Here, we discuss the effect of the QBO on the age spectrum. QBO-related inter-annual variability of mean age has recently been shown to be well represented in the ERA-Interim driven CLaMS simulation used here, if compared to Michelson Interferometer for Passive Atmospheric Sounding (MIPAS) observations (Ploeger et al., 2015b, Fig. 1).

The QBO is known to induce a secondary meridional circulation with anomalous upwelling in the tropics during easterly shear phase and anomalous downwelling during westerly shear phase (e.g., Baldwin et al., 2001). Figure 12 shows composites of the tropical age spectrum at 600 K, calculated by averaging all age spectra in that region for 1989–2013 during periods when the corresponding zonal mean zonal wind was greater than 10 m/s versus less than -10 m/s (defining westerly/easterly QBO composites, respectively). The limit of ± 10 m/s has been chosen to enhance the clarity of the differences between the two composites. Relaxing the limit to 0 m/s results in qualitatively the same conclusions. Consistent with faster QBO-induced upwelling, the easterly QBO composite results in an age spectrum skewed towards shorter transit times, with modal age and mean age about 0.5 years younger as compared to the westerly QBO composite. Likewise, RCTT's are shorter during easterly QBO phase by ≈ 0.3 yr. Furthermore the spectrum shape differs between the two composites. During easterly QBO phase the tropical age spectrum shows a mono-modal shape, whereas secondary peaks develop during westerly QBO phase. These secondary peaks at older transit times (here 2.5, 3.5, 4.5 years) indicate an increased impact of in-mixing of old extratropical air on the tropical composition, consistent with enhanced subtropical mixing during westerly QBO phase (e.g., Shuckburgh et al., 2001; Abalos et al., 2016). This enhanced mixing results from shifts in the critical lines, allowing Rossby waves to propagate further equatorward and into the tropics.

Figure 13 (left panels) shows the time series of simulated age spectra in the lower stratosphere at 600 K for the tropics (a) and extratropics of both hemispheres (c/e). The tropical spectra (Fig. 13a–b) at 600 K show the strong QBO-related inter-annual variability, as discussed above. Comparing the respective deseasonalized age spectrum anomalies (constructed by subtracting the mean annual cycle at each transit time) to tropical zonal mean zonal wind (red bars highlight easterly wind periods) confirms that, indeed, the clearest mode of inter-annual variability is related to the QBO, with increased fractions of young air during QBO easterly phases, and opposite behaviour during QBO westerly phases. Furthermore, the modal age (white diamonds) varies between one and two years, with inter-annual variations closely matching the variability in RCTT (red line).

This highlights the dominant influence of the residual circulation on transport variations in the tropical lower stratosphere on inter-annual time scales. Even the inter-annual variations of mean age (black line) closely follow those of the RCTT (Fig. 13b). A discontinuity in the tropical age spectrum time series at the end of 1993 (most strongly evident in panel b) could hint at problems with the reanalysis data, but we were not able to relate it to specific changes in the assimilation system.

5 Also the extratropical age spectra show strong QBO-related inter-annual variations in both hemispheres (Fig. 13c–f). The fraction of young air increases at the end of QBO easterly phases, lagging the tropical signal by a few months. Remarkably, these young air peaks originating in QBO easterly phases propagate to older transit times and determine the modal age during the following 2–3 years. For example, the modal age during 1996–1999 is set in the easterly QBO phase in 1996 (see Fig. 13c). Analogous behaviour results from QBO westerly phases, with anomalously old air originating in the tropics and being
10 transported poleward. Clearly, the tropical air affected by anomalous transport during a specific QBO phase subsequently circulates around and may leave the stratosphere. However, the propagation of the signal shows the remarkable fact that enough of the air recirculates back to preserve the memory of the original signal over the 2-3 following years. The propagation of the modal age along the transit time axis clearly shows how the QBO affects the composition of the lower stratosphere on a global scale. Inter-annual variability on the 400 K isentropic surface implies modulations due to the El Niño Southern Oscillation
15 (ENSO, not shown), although not as conclusively as the modulations due to the QBO.

6 Discussion

As mentioned already in the introduction, different explanations have been proposed for the occurrence of multiple peaks in seasonal age spectra. Bönisch et al. (2009) refined the work by Andrews et al. (2001) and assumed that age spectra in the lowermost stratosphere (below about 380 K) result from the superposition of two single peak spectra, related to a fast
20 (quasi-horizontal mixing and shallow circulation branch) and a slow pathway (deep circulation branch). They noted that this superposition does not necessarily cause a bimodal spectrum shape for sufficiently strong overlap of the individual spectra. Reithmeier et al. (2007) found several peaks in their age spectra, but only at polar latitudes. They explained these peaks as resulting from the annual cycle in tropical upward mass flux into the stratosphere, maximizing during NH winter, and the seasonal variation in the polar vortex transport barrier, allowing horizontal transport to high latitudes only in spring and summer.
25 This results in the superposition of single mode spectra from low latitudes once per year. Li et al. (2012a) also found multi-peak age spectra in their model simulation at polar latitudes, but conversely to Reithmeier et al. (2007) argued that these peaks form mainly due to the fact that air masses leaving the boundary layer during NH summer would have the highest probability to recirculate into the polar stratosphere.

As indicated in Fig. 9, we find multiple peaks as a generic feature throughout the lower stratosphere, although these peaks are
30 most pronounced at high latitudes. Closer inspection of the peaks shows that they correspond to NH winter pulse release times (cf. peaks in the BIR map in Fig. 3a). To further highlight this point, Fig. 14a presents the distribution of the source times of the age spectrum peaks, hence the time when the air corresponding to the peaks has left the boundary source region at the Earth's surface. The clear maximum at NH winter source times shows that the air corresponding to the peaks has left the surface layer

during NH winter. Note that the figure shows the distribution of surface source times for air parcels sampled in the stratosphere – the pulse release rate at the surface is not varying. Figure 14b further shows that also for the full age spectrum (not only the peaks) air leaving the boundary surface during NH winter is most likely. For example, about twice as much stratospheric air has left the surface in January compared to May. The link of the age spectrum peaks to an enhanced probability of stratospheric air to originate at the surface during NH winter explains also the occurrence of the peaks at approximately the same transit time independent of latitude and level (Fig. 9), and is consistent with the interpretation by Reithmeier et al. (2007).

One explanation for the enhanced occurrence of NH winter surface air in the spectrum is that air parcels preferentially enter the stratosphere during NH winter (cf. argument in Reithmeier et al., 2007). Another possible explanation is that vertical lofting in the tropical stratosphere only occurs efficiently during NH winter when tropical upwelling is strongest and the tropical stratosphere is well isolated. Some of this air then reaches the region of interest through a more or less direct pathway. Some of it recirculates and reaches the region in following years. Pulses released during NH spring and summer, on the other hand, are efficiently dispersed meridionally before they reach the tropical pipe and therefore are less likely to undergo recirculation in the stratosphere. This is consistent with a stronger return flux into the troposphere for air entering the stratosphere in July compared to January (Orbe et al., 2014). A sensitivity calculation with pulses released at the tropical tropopause (not shown) also results in age spectra with annually repeating peaks, however weaker. Therefore, a combination of all transport processes described above likely plays a role.

At first glance, the aging of the peaks by 1 month per month at a given location in the stratosphere (e.g. Fig. 6) would be consistent with air simply staying at that location. This is possible in the extratropical middle and upper stratosphere during summer where the circulation essentially shuts down. But it is inconsistent with the aging of the peaks throughout the year - during winter the air is expected to sink, for example. Hence, the propagation of the peaks to older transit times (Fig. 6) results from the interplay of various processes.

Figure 9 shows that maximum tropical upward mass flux during NH winter causes a strong peak at short transit times in the tropical lower stratosphere age spectrum. This tropical young air is transported rapidly by isentropic mixing and the shallow circulation branch to middle and high latitudes during spring and summer when the subtropical jet transport barrier is weak and the polar vortex transport barrier is absent. Therefore, the young air peak extends from the tropics to the summer pole (see Fig. 9a–b), particularly in the NH. A fraction of the tropical air, however, is transported through the deep circulation branch and arrives at higher latitudes later (e.g., during the following winters, when the deep circulation branch is most active). The comparison between air originating at the surface during winter with air originating at the surface during summer after 3 years of being transported through the atmosphere in Fig. 2 (right panels) shows that particularly at higher levels in the stratosphere winter surface air is more prevalent. As this air corresponds to the same winter source time as the air which was transported directly to higher latitudes at lower levels, it effectively creates the age spectrum peak at older transit times and compensates the diluting effect of downwelling. Some of the extratropical air recirculates into the tropics and amplifies the peaks in the spectrum tail. As the deep circulation branch is strongest during NH winter, the older spectrum peaks appear stronger in winter than summer (e.g., Fig. 9a–b). Mixing causes attenuation of the peaks.

Other modes of variability in transport, such as the QBO, may also modify the shape of the age spectrum and the occurrence of multiple peaks (see Fig. 13 and related discussion). Remarkably, the age spectrum mode may remain attached to one specific QBO phase for several years, with similar behaviour also possible for other modes of inter-annual variability. The existence of a shallow and fast transport pathway further affects the shape of age spectra in the lowermost stratosphere. Transport by the deep circulation branch is likely responsible for the amplification of the older peaks at high latitudes (Fig. 9), but is not creating an additional peak, in agreement with Bönisch et al. (2009).

In contrast to Reithmeier et al. (2007) and Li et al. (2012a), the CLaMS age spectrum peaks are more pronounced, with multiple peaks occurring also in the subtropics and mid-latitudes, and even weakly so in the tropics (e.g., Figs. 9, 12). Problems with representing the subtropical transport barrier in ECHAM4 (see Reithmeier et al., 2007) likely caused a masking of the multiple peaks at these latitudes in their study. Li et al. (2012a) used a climate model (GEOSCCM) that likely contained stronger numerical diffusion compared to the Lagrangian transport model used here. On the other hand, CLaMS is driven by reanalysis winds, which are known to be overly dispersive (Schoeberl et al., 2003). A detailed understanding of the differences in the occurrence of multiple spectral peaks at lower latitudes in different models requires further work.

In summary, multiple peaks are a generic characteristic of age spectra in the lower stratosphere and are caused by seasonality and inter-annual variability in transport. Hence, an accurate fit of age spectra in the lower stratosphere requires the superposition of a number of 1D diffusion Green's functions, with this number equal to the number of distinct peaks in the spectrum. We tested such a fitting procedure and found that it works well.

7 Conclusions

We presented seasonally and inter-annually varying age spectra in the lower stratosphere calculated with the Lagrangian transport model CLaMS driven by ERA-Interim winds for the period 1979-2013. Our approach is based on the boundary impulse response (BIR) method (e.g., Haine et al., 2008; Li et al., 2012a), generalized to transient simulations using quasi-observational winds, and is therefore more appropriately termed the Boundary Impulse (time-)Evolving Response (BIER) method.

Seasonal age spectra in the lower stratosphere show large deviations from an idealized stationary uni-modal shape. Multiple peaks emerge in the age spectra throughout the stratosphere (strongest at high latitudes), caused by the interplay of seasonally varying tropical upwelling, stratospheric transport barriers and recirculation. These multiple peaks are largely related to the fact that air entering the stratosphere during NH winter makes up the biggest fraction throughout the stratosphere. While the annual mean spectrum is in large parts well described by a Green's function representative of idealized stationary transport, seasonal age spectra with multiple peaks can only be well approximated by a superposition of such functions. In addition to seasonality, inter-annual variations in transport (e.g., QBO) cause significant age spectrum modulations. Stronger upwelling during easterly QBO phase increases the fraction of young air in the spectrum. We found that one specific QBO phase may determine the modal age (age spectrum maximum) for up to 3 years across a wide range of latitudes.

Interpretation of the age spectrum in terms of residual circulation and mixing is not straightforward, with different effects dominating in different atmospheric regions. We found residual circulation trajectories, which are much more easily obtained

than age spectra or even mean age, to represent a good approximation of the dominant pathway in the deep tropics and in the winter extratropics above about 500 K, as represented by the modal age in these regions. In contrast, eddy mixing strongly modifies the modal age in summer, particularly in the lowermost stratosphere.

Analysis of the full age spectrum compared to mean age is advantageous for separating the effects of different transport processes, as has been already emphasized in earlier studies (e.g., Hall, 1999; Waugh and Hall, 2002). In this sense, knowledge of the exact fractions of air masses with certain transit times, as included in the full age spectrum, is highly beneficial for a more detailed understanding of stratospheric chemistry and composition. Including time-dependent age spectrum diagnostics in state-of-the-art atmospheric climate and transport models would help to avoid ambiguities in model inter-comparisons of stratospheric transport.

10 Appendix A: Correction for finite age spectrum tail

The tail of the age spectrum $G(\tau)$ in the lower stratosphere generally decreases exponentially at transit times larger than about 4-5 years (e.g, Fig. 3c), as noted by several authors (e.g., Reithmeier et al., 2007; Diallo et al., 2012; Li et al., 2012a). At large transit times $\tau > \tau^*$, larger than some threshold τ^* , the spectrum tail may therefore be approximated by an exponential function to define a *corrected age spectrum* by

$$15 \quad G_{\text{corr}}(\tau) = \begin{cases} G(\tau) & \text{for } \tau \leq \tau^* \\ G(\tau^*) e^{-\frac{\tau}{\xi}} & \text{for } \tau > \tau^* . \end{cases} \quad (\text{A1})$$

As our multi-pulse set-up in CLaMS with 60 pulse tracers every two months (see Sect. 2.2) allows calculating the age spectrum for transit times up to ten years, we chose $\tau^* = 10$ years and determine the decay time scale ξ by fitting the exponential function for transit times $5 \text{ yr} < \tau < 10 \text{ yr}$.

Integration of the corrected age spectrum (Eq. A1) over transit time (from zero to infinity) yields the corrected norm and the first moment of the age spectrum (the corrected mean age) (see also Diallo et al., 2012, Eq. 2)

$$N_{\text{corr}} = N + G(\tau^*) \xi , \quad (\text{A2})$$

$$\Gamma_{\text{corr}} = \Gamma^* + G(\tau^*) \xi (t^* + \xi) . \quad (\text{A3})$$

Figure 15 shows the reference (uncorrected) mean age from the CLaMS climatological age spectrum for winter and summer and the difference to the corrected mean age (corrected minus reference). As expected, the correction of the spectrum tail up to infinite transit times causes older mean age globally. The differences increase with increasing latitude and altitude, remaining less than about 6 months throughout large parts of the lower stratosphere, but increasing to about 1 year inside the polar vortex (particularly in the SH).

An interesting side note concerns the comparison with the ‘clock-tracer’ age, which is younger than the corrected (but older than the uncorrected) age spectrum mean age (Fig. 4). From theoretical considerations based on stationary flow (Hall and Haine, 2002, Eq. 9) showed that ‘ideal age’ (an alternate for the ‘clock-tracer’ used here) converges faster to a steady-state value than

the spectrum mean age, which seems at first glance contradictory to the comparison between ‘clock-tracer’ and corrected spectrum mean age presented here. However, there is no contradiction as the time span for convergence is not directly comparable. The ‘clock-tracer’ was subject to a 10 year spin-up (repeating 1979 conditions) plus 10 years of transient simulation (1979-1988) before taking it into consideration, whereas the age spectrum has explicitly been calculated over 10 years of transit time
5 (1979-1988 simulation) but with the tail fitted to infinite transit times, as explained above. Hence, the effective calculation length is longer for the corrected age spectrum than for the ‘clock-tracer’.

Acknowledgements. We thank John Bergman, Harald Bönisch, Paul Konopka and Bernard Legras for helpful discussions and suggestions. Thanks also to Nicole Thomas for programming support and to the ECMWF for providing reanalysis data. This work was funded by the German Federal Ministry of Education and Research (BMBF) within the “ROMIC” programme under project 01LG1222A. Felix Ploeger
10 was funded by a HGF postdoc grant.

References

- Abalos, M., Legras, B., Ploeger, F., and Randel, W. J.: Evaluating the advective Brewer-Dobson circulation in three reanalyses for the period 1979–2012, *J. Geophys. Res.*, 120, doi:10.1002/2015JD023182, 2015.
- Abalos, M., Legras, B., and Shuckburgh, E.: Interannual variability in effective diffusivity in the upper troposphere/lower stratosphere from reanalysis data, *Q. J. R. Meteorol. Soc.*, doi:10.1002/qj.2779, 2016.
- Andrews, A. E., Boering, K. A., Wofsy, S. C., Daube, B. C., Jones, D. B., Alex, S., Loewenstein, M., Podolske, J. R., and Strahan, S. E.: Empirical age spectra for the midlatitude lower stratosphere from in situ observations of CO₂: Quantitative evidence for a subtropical “barrier” to horizontal transport, *J. Geophys. Res.*, 106, D10, 2001.
- Andrews, D. G., Holton, J. R., and Leovy, C. B.: *Middle Atmosphere Dynamics*, Academic Press, San Diego, USA, 1987
- Baldwin, M. P., Gray, L. J., Dunkerton, T. J., Hamilton, K., Haney, P. H., Randel, W. J., Holton, J. R., Alexander, M. J., Hirota, I., Horinouchi, T., Jones, D. B. A., Kinnersley, J. S., Marquardt, C., Sato, K., and Takahashi, M.: The quasi-biennial oscillation, *Rev. Geophys.*, 39, 179–229, doi:10.1029/1999RG000073, 2001.
- Birner, T. and Bönisch, H.: Residual circulation trajectories and transit times into the extratropical lowermost stratosphere, *Atmos. Chem. Phys.*, 11, 817–827, doi:10.5194/acp-11-817-2011, 2011.
- Bönisch, H., Engel, A., Curtius, J., Birner, T., and Hoor, P.: Quantifying transport into the lowermost stratosphere using simultaneous in-situ measurements of SF₆ and CO₂, *Atmos. Chem. Phys.*, 10, 5905–5919, 2009.
- Bönisch, H., Engel, A., Birner, T., Hoor, P., Tarasick, D. W., and Ray, E. A.: On the structural changes in the Brewer-Dobson circulation after 2000, *Atmos. Chem. Phys.*, 11, 3937–3948, doi:10.5194/acp-11-3937-2011, 2011.
- Butchart, N.: The Brewer-Dobson circulation, *Rev. Geophys.*, 52, 157–184, doi:10.1002/2013RG000448, 2014.
- Butchart, N., Cionni, I., Eyring, V., Shepherd, T. G., Waugh, D. W., Akiyoshi, H., Austin, J., Brühl, C., Chipperfield, M. P., Cordero, E., Dameris, M., Deckert, R., Dhomse, S., Frith, S. M., Garcia, R. R., Gettelman, A., Giorgetta, M. A., Kinnison, D. E., Li, F., Mancini, E., McLandress, C., Pawson, S., Pitari, G., Plummer, D. A., Rozanov, E., Sassi, F., Scinocca, J. F., Shibata, K., Steil, B., and Tian, W.: Chemistry–Climate Model Simulations of Twenty–First Century Stratospheric Climate and Circulation Changes, *J. Climate*, 23, 5349–5374, doi:10.1175/2010JCLI3404.1, 2010.
- Calvo, N., Garcia, R. R., Randel, W. J., and Marsh, D. R.: Dynamical Mechanism for the Increase in Tropical Upwelling in the Lowermost Tropical Stratosphere during Warm ENSO Events, *J. Atmos. Sci.*, 67, 2331–2340, 2010.
- Dee, D. P., Uppala, S. M., Simmons, A. J., Berrisford, P., Poli, P., Kobayashi, S., Andrae, U., Balmaseda, M. A., Balsamo, G., Bauer, P., Bechtold, P., Beljaars, A. C. M., van de Berg, L., Bidlot, J., Bormann, N., Delsol, C., Dragani, R., Fuentes, M., Geer, A. J., Haimberger, L., Healy, S. B., Hersbach, H., Holm, E. V., Isaksen, L., Kallberg, P., Kohler, M., Matricardi, M., McNally, A. P., Monge-Sanz, B. M., Morcrette, J. J., Park, B. K., Peubey, C., de Rosnay, P., Tavolato, C., Thepaut, J. N., and Vitart, F.: The ERA-Interim reanalysis: configuration and performance of the data assimilation system, *Q. J. R. Meteorol. Soc.*, 137, 553–597, doi:10.1002/qj.828, 2011.
- Diallo, M., Legras, B., and Chedin, A.: Age of stratospheric air in the ERA-Interim, *Atmos. Chem. Phys.*, 12, 12 133–12 154, 2012.
- Ehhalt, D. H., Rohrer, F., Schauffler, S., and Prather, M.: On the decay of stratospheric pollutants: Diagnosing the longest-lived eigenmode, *J. Geophys. Res.*, 109, 347–350, doi:10.1029/2003JD004029, 2004.
- Engel, A., Möbius, T., Bönisch, H.-P., Schmidt, U., Heinz, R., Levin, I., Atlas, E., Aoki, S., Nakazawa, T., Sugawara, S., Moore, F., Hurst, D., Elkins, J., Schauffler, S., Andrews, A., and Boering, K.: Age of stratospheric air unchanged within uncertainties over the past 30 years, *Nat. Geosci.*, 2, 28–31, doi:10.1038/NGEO388, 2009.

- Garny, H., Dameris, M., Randel, W. J., Bodeker, G. E., and Deckert, R.: Dynamically Forced Increase of Tropical Upwelling in the Lower Stratosphere, *J. Atmos. Sci.*, 68, 1214–1233, doi:10.1175/2011JAS3701.1, 2011.
- Garny, H., Birner, T., Bönisch, H., and Bunzel, F.: The effects of mixing on age of air, *J. Geophys. Res.*, 119, doi:10.1002/2013JD021417, 2014.
- 5 Haenel, F., Stiller, G. P., von Clarmann, T., Funke, B., Eckert, E., Glatthor, N., Grabowski, U., Kellmann, S., Kiefer, M., Linden, A., and Reddmann, T.: Reassessment of MIPAS age of air trends and variability, *Atmos. Chem. Phys.*, 22, 13161–13176, 2015.
- Haine, T. W. N., Zhang, H., Waugh, D. W., and Holzer, M.: On transit time distributions in unsteady circulation models, *Ocean Mod.*, 21, 35–45, 2008.
- Hall, T. M. and Plumb, R. A.: Age as a diagnostic of stratospheric transport, *J. Geophys. Res.*, 99, 1059–1070, 1994.
- 10 Hall, T. M.: Evaluation of transport in stratospheric models, *J. Geophys. Res.*, 104 (D14), 18815–18839, 1999.
- Hall, T. M. and Haine, T. W. N.: On Ocean Transport Diagnostics: The Idealized Age Tracer and the Age Spectrum, *J. Phys. Oceanogr.*, 32, 1987–1991, 2002.
- Haynes, P. and Shuckburgh, E.: Effective diffusivity as a diagnostic of atmospheric transport 1. Stratosphere, *J. Geophys. Res.*, 105, 22 777–22 794, 2000.
- 15 Haynes, P., Marks, C. J., McIntyre, M. E., Shepherd, T. G., and Shine, K. P.: On the downward control of extratropical diabatic circulations by eddy-induced mean zonal forces, *J. Atmos. Sci.*, 48, 651–679, 1991.
- Hegglin, M. I. and Shepherd, T. G.: O₃-N₂O correlations from the Atmospheric Chemistry Experiment: Revisiting a diagnostic of transport and chemistry in the stratosphere, *J. Geophys. Res.*, D19301, doi:10.1029/2006JD008281, 2007.
- Holton, J. R., Haynes, P., McIntyre, M. E., Douglass, A. R., Rood, R. B., and Pfister, L.: Stratosphere-troposphere exchange, *Rev. Geophys.*, 20 33, 403–439, 1995.
- Holzer, M. and Hall, T. M.: Transit-time and tracer-age distributions in geophysical flows, *J. Atmos. Sci.*, 57, 3539–3558, 2000.
- Konopka, P., Steinhorst, H.-M., Groöß, J.-U., Günther, G., Müller, R., Elkins, J. W., Jost, H.-J., Richard, E., Schmidt, U., Toon, G., and McKenna, D. S.: Mixing and Ozone Loss in the 1999–2000 Arctic Vortex: Simulations with the 3-dimensional Chemical Lagrangian Model of the Stratosphere (CLaMS), *J. Geophys. Res.*, 109, D02315, doi:10.1029/2003JD003792, 2004.
- 25 Konopka, P., Ploeger, F., Tao, M., Birner, T., and Riese, M.: Hemispheric asymmetries and seasonality of mean age of air in the lower stratosphere: Deep versus shallow branch of the Brewer-Dobson circulation, *J. Geophys. Res.*, doi:10.1002/2014JD022429, 2015.
- Li, F., Waugh, D. W., Douglass, A. R., Newman, P. A., Pawson, S., Stolarski, R. S., Strahan, S. E., and Nielsen, J. E.: Seasonal variations in stratospheric age spectra in GEOSCCM, *J. Geophys. Res.*, 117, D5, doi:10.1029/2011JD016877, 2012a.
- Li, F., Waugh, D. W., Douglass, A. R., Newman, P. A., Strahan, S. E., Ma, J., Nielsen, J. E., and Liang, Q.: Long-term changes in stratospheric age spectra in the 21st century in the Goddard Earth Observing System Chemistry-Climate Model (GEOSCCM), *J. Geophys. Res.*, 117, D20, doi:10.1029/2012JD017905, 2012b.
- Mahowald, N. M., Plumb, R. A., Rasch, P. J., del Corral, J., and Sassi, F.: Stratospheric transport in a three-dimensional isentropic coordinate model, *J. Geophys. Res.*, 107, D15, doi:10.1029/2001JD001313, 2002.
- McKenna, D. S., Konopka, P., Groöß, J.-U., Günther, G., Müller, R., Spang, R., Offermann, D., and Orsolini, Y.: A new Chemical Lagrangian Model of the Stratosphere (CLaMS): 1. Formulation of advection and mixing, *J. Geophys. Res.*, 107, 4309, doi:10.1029/2000JD000114, 2002.
- 30 Orbe, C., Holzer, M., Polvani, L. M., and Waugh, D. W.: Air-mass origin as a diagnostic of tropospheric transport, *J. Geophys. Res.*, 118, 1459–1470, doi:10.1002/jgrd.50133, 2013.

- Orbe, C., Holzer, M., Polvani, L. M., Waugh, D. W., Li, F., Oman, L. D., and Newman, P. A.: Seasonal ventilation of the stratosphere: Robust diagnostics from one-way flux distributions, *J. Geophys. Res.*, 119, 293–306, doi:10.1002/2013JD020213, 2014.
- Ploeger, F., Abalos, M., Birner, T., Konopka, P., Legras, B., Müller, R., and Riese, M.: Quantifying the effects of mixing and residual circulation on trends of stratospheric mean age of air, *Geophys. Res. Lett.*, 42, 2047–2054, doi:10.1002/2014GL062927, 2015a.
- 5 Ploeger, F., Riese, M., Haanel, F., Konopka, P., Müller, R., and Stiller, G.: Variability of stratospheric mean age of air and of the local effects of residual circulation and eddy mixing, *J. Geophys. Res.*, 120, 716–733, doi:10.1002/2014JD022468, 2015b.
- Plumb, R. A. and Ko, M. K. W.: Interrelationships between mixing ratios of long-lived stratospheric constituents, *J. Geophys. Res.*, 97, 10 145–10 156, 1992.
- Plumb, R. A.: A “tropical pipe” model of stratospheric transport, *J. Geophys. Res.*, 101, 3957–3972, 1996.
- 10 Pommrich, R., Müller, R., Groß, J.-U., Konopka, P., Ploeger, F., Vogel, B., Tao, M., Hoppe, C. M., Günther, G., Spelten, N., Hoffmann, L., Pumphrey, H.-C., Viciani, S., D’Amato, F., Volk, C. M., Hoor, P., Schlager, H., and Riese, M.: Tropical troposphere to stratosphere transport of carbon monoxide and long-lived trace species in the Chemical Lagrangian Model of the Stratosphere (CLaMS), *Geosci. Model Dev.*, 7, 2895–2916, 2014.
- Randel, W. J., Garcia, R. R., Calco, N., and Marsh, D.: ENSO influence on zonal mean temperature and ozone in the tropical lower strato-
 15 sphere, *Geophys. Res. Lett.*, 36, L15822, doi:10.1029/2009GL039343, 2009.
- Randel, W. J., Park, M., Emmons, L., Kinnison, D., Bernath, P., Walker, K. A., Boone, C., and Pumphrey, H.: Asian Monsoon Transport of Pollution to the Stratosphere, *Science*, 328, 611–613, doi:10.1126/science.1182274, 2010.
- Ray, E. A., et al. (2010), Evidence for changes in stratospheric transport and mixing over the past three decades based on multiple data sets and tropical leaky pipe analysis, *J. Geophys. Res.*, 115, D21304.
- 20 Ray, E. A., Moore, F. L., Rosenlof, K. H., Davis, S. M., Sweeney, C., Tans, P., Wang, T., Elkins, J. W., Boenisch, H., Engel, A., Sugawara, S., Nakazawa, T., and Aoki, S.: Improving stratospheric transport trend analysis based on SF₆ and CO₂ measurements, *J. Geophys. Res.*, 119, 14 110–14 128, 2014.
- Reithmeier, C., Sausen, R., and Grewe, V.: Investigating lower stratospheric model transport: Lagrangian calculations of mean age and age spectra in the GCM ECHAM4, *Clim. Dynamics*, 30, 225–238, 2008.
- 25 Riese, M., Ploeger, F., Rap, A., Vogel, B., Konopka, P., Dameris, M., and Forster, P. M.: Impact of uncertainties in atmospheric mixing on simulated UTLS composition and related radiative effects, *J. Geophys. Res.*, 117, D16, doi:10.1029/2012JD017751, 2012.
- Rosenlof, K. H.: Seasonal cycle of the residual mean meridional circulation in the stratosphere, *J. Geophys. Res.*, 100, 5173–5191, 1995.
- Schoeberl, M. R., Douglass, A. R., Zhu, X. S., and Pawson, S.: A comparison of the lower stratospheric age spectra derived from a general circulation model and two data assimilation systems, *J. Geophys. Res.*, 108, D3, 2003.
- 30 Schoeberl, M. R., Douglass, A. R., Polansky, B., Boone, C., Walker, K. A., and Bernath, P.: Estimation of stratospheric age spectrum from chemical tracers, *J. Geophys. Res.*, 110, D21, 2005.
- Seviour, W. J. M., Butchart, N., and Hardiman, S. C.: The Brewer-Dobson circulation inferred from ERA-Interim, *Q. J. R. Meteorol. Soc.*, 138, 878–888, 2011.
- Shuckburgh, E., Norton, W., Iwy, A., and Haynes, P.: Influence of the quasi-biennial oscillation on isentropic transport and mixing in the
 35 tropics and subtropics, *J. Geophys. Res.*, 116, D13, 2001.
- Solomon, S., Rosenlof, K. H., Portmann, R. W., Daniel, J., Davis, S. M., Sanford, T. J., and Plattner, G. K.: Contributions of Stratospheric Water Vapor to Decadal Changes in the Rate of Global Warming, *Science*, 327, 1219–1223, 2010.

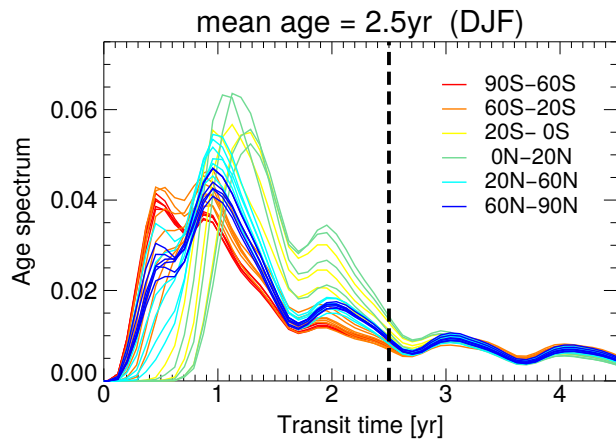


Figure 1. Climatological age spectra for the same mean age of 2.5 years but at different latitude ranges, for December–February. Each line is the average over DJF, with different age spectra of the same color representing different latitudes within the respective latitude band. The black dashed line highlights the mean age of 2.5 years.

Stiller, G. P., von Clarmann, T., Haanel, F., Funke, B., Glatthor, N., Grabowski, U., Kellmann, S., Kiefer, M., Linden, A., Lossow, S., and López-Puertas, M.: Observed temporal evolution of global mean age of stratospheric air for the 2002 to 2010 period, *Atmos. Chem. Phys.*, 12, 3311–3331, 2012.

5 Volk, C. M., Elkins, J. W., Fahey, D. W., Salawitch, R. J., Dutton, G. S., Gilligan, J. M., Proffitt, M. H., Loewenstein, M., Podolske, J. R., Minschwaner, K., Margitan, J. J., and Chan, K. R.: Quantifying transport between the tropical and mid-latitude lower stratosphere, *Science*, 272, 1763–1768, 1996.

Waugh, D. W. and Hall, T. M.: Age of stratospheric air: Theory, observations, and models, *Rev. Geophys.*, 40, 1–27, 2002.

10 Wolter, K. and Timlin, M.: Monitoring ENSO in COADS with a seasonally adjusted principal component index, in: Proc. of the 17th Climate Diagnostics Workshop, Norman, OK, NOAA/NMC/CAC, NSSL, Oklahoma Clim. Survey, CIMMS and the School of Meteor., Univ. of Oklahoma, pp. 52–57, 1993.

Wolter, K. and Timlin, M.: Measuring the strength of ENSO events - how does 1997/98 rank?, *Weather*, 53, 315–324, 1998.

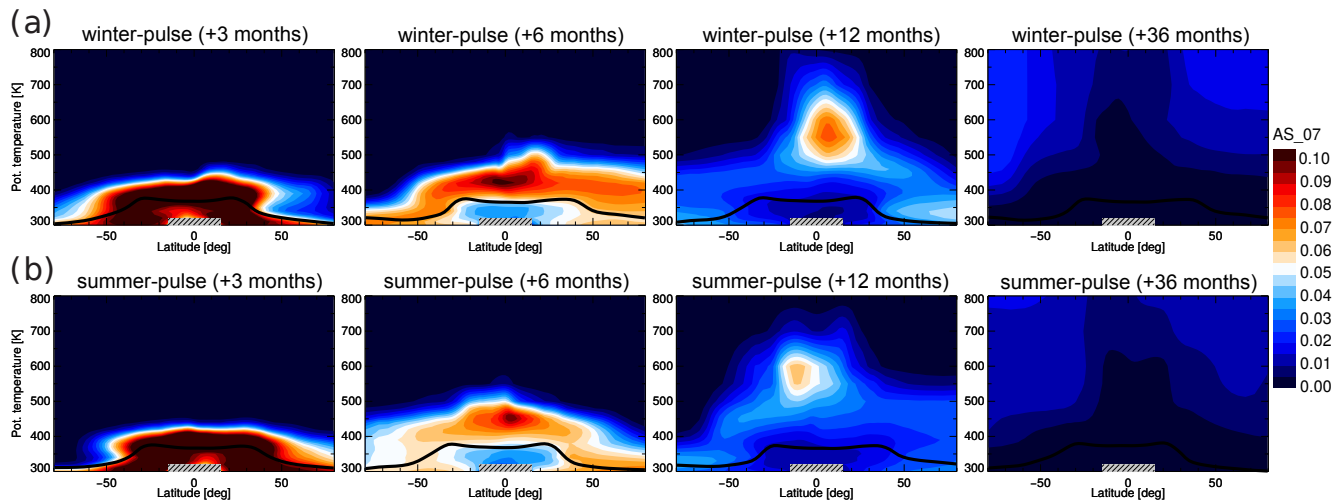


Figure 2. Evolution of tracer pulses released in the tropical boundary layer during NH winter (a) and summer (b) during the following months (3, 6, 12, 36 months after pulse release). The winter pulse was released during January 2000, the summer pulse during July 2000. The black line shows the climatological tropopause, the grey hatched line at the tropical surface the pulse release region.

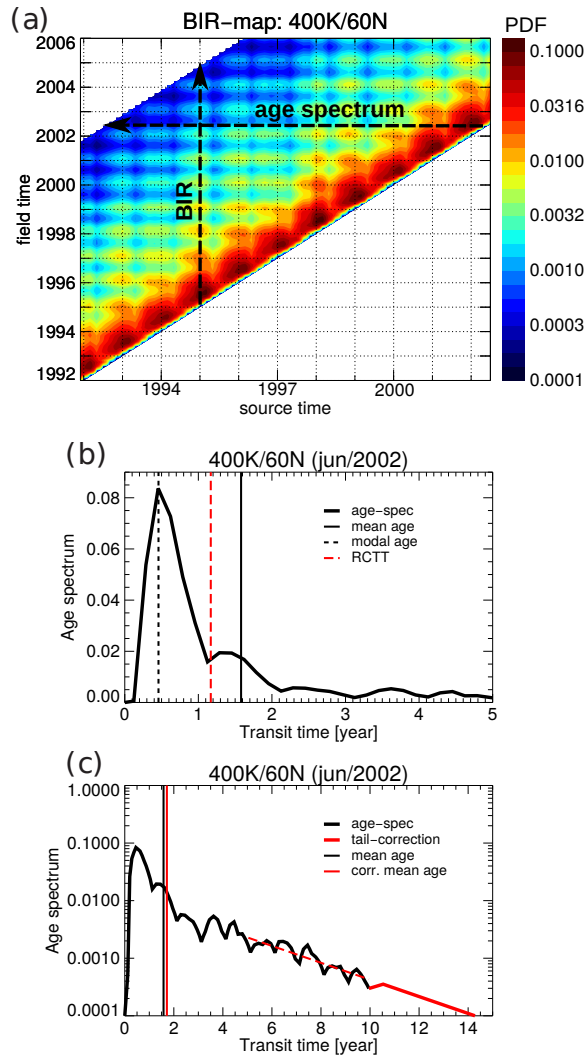


Figure 3. (a) BIR map from CLaMS pulse tracers at 400 K and 60°N, plotted only for part of the full simulation period. Arrows highlight vertical and horizontal cuts through the BIR map representing BIR (vertical) and age spectrum (horizontal), respectively (cf. Haine et al., 2008). (b) The age spectrum for June 2002, corresponding to the horizontal cut in (a). Vertical lines show mean age (solid), modal age (black dashed) and the residual circulation transit time (red dashed, see text). (c) Same as (b), but including a correction for the finite spectrum tail using an exponential fit (see text). The red vertical line shows mean age for the tail-corrected spectrum, the black line for the uncorrected case (Note the larger transit time range and logarithmic y-axis).

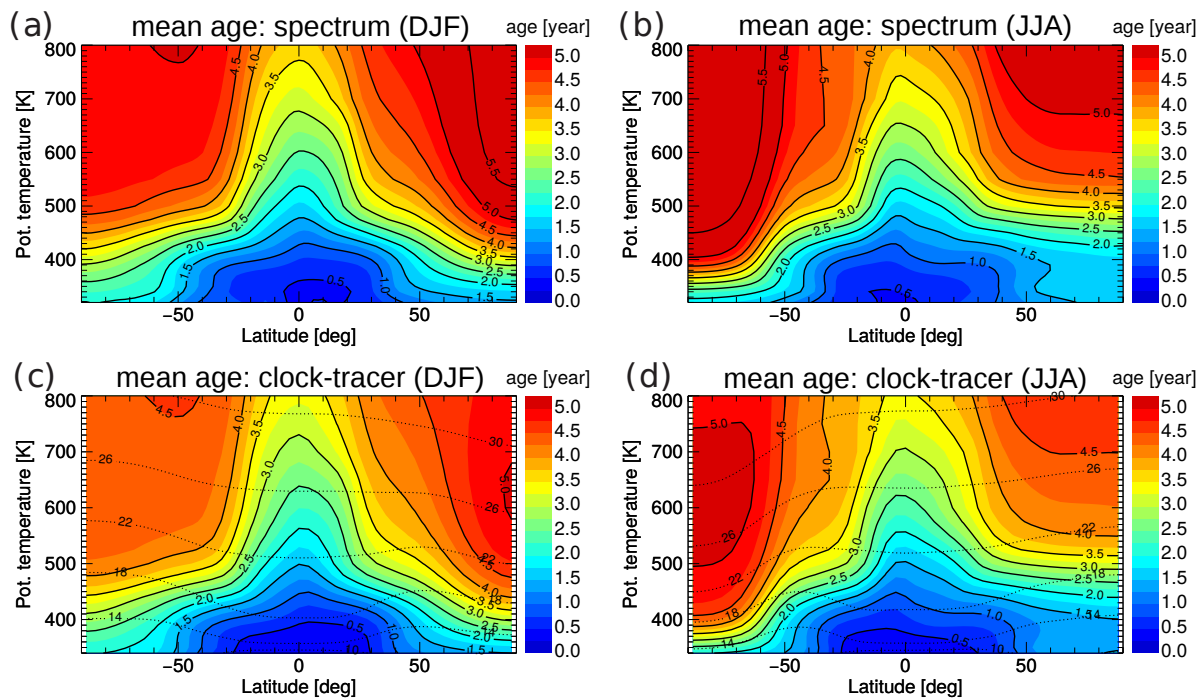


Figure 4. Mean age from the 1989–2013 CLaMS age spectrum climatology for (a) December–February and (b) June–August. Corresponding mean ages calculated from the model’s ‘clock-tracer’ are shown in (c) and (d) for comparison. Black dotted lines in (c/d) show altitude levels in km for reference.

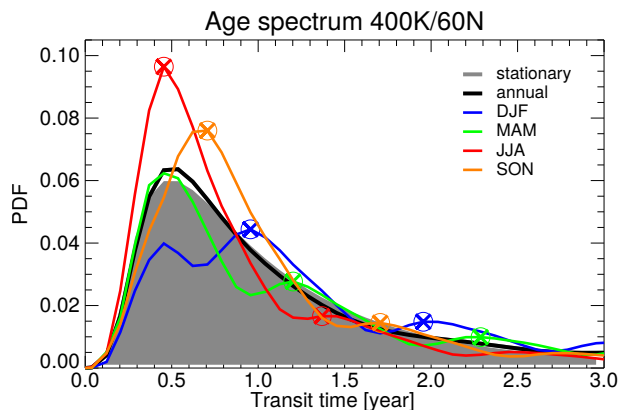


Figure 5. Seasonality of the climatological age spectrum at 400 K in NH mid-latitudes (60°N). The annual mean spectrum is shown as a black thick line, the idealized stationary shape (see text) as grey shading, and different seasons as coloured lines. Symbols illustrate the evolution of the peak (see text for details).

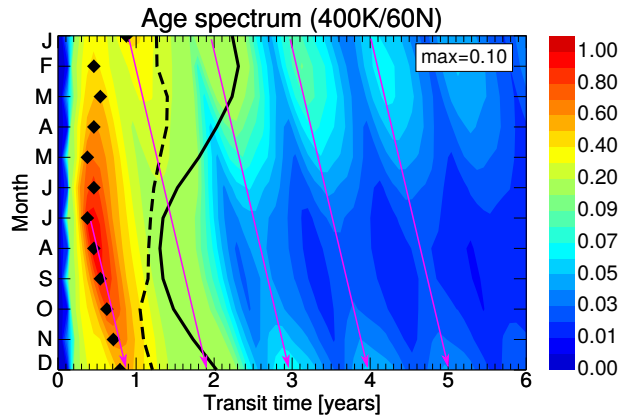


Figure 6. Seasonal cycle of the climatological age spectrum at 400 K in the NH extratropics (60°N). Mean age is shown as black thick line, modal age as black symbols, and RCTT as black dashed line. The pink arrows illustrate the time evolution of the spectrum peaks. (Note the non-linear colour scale).

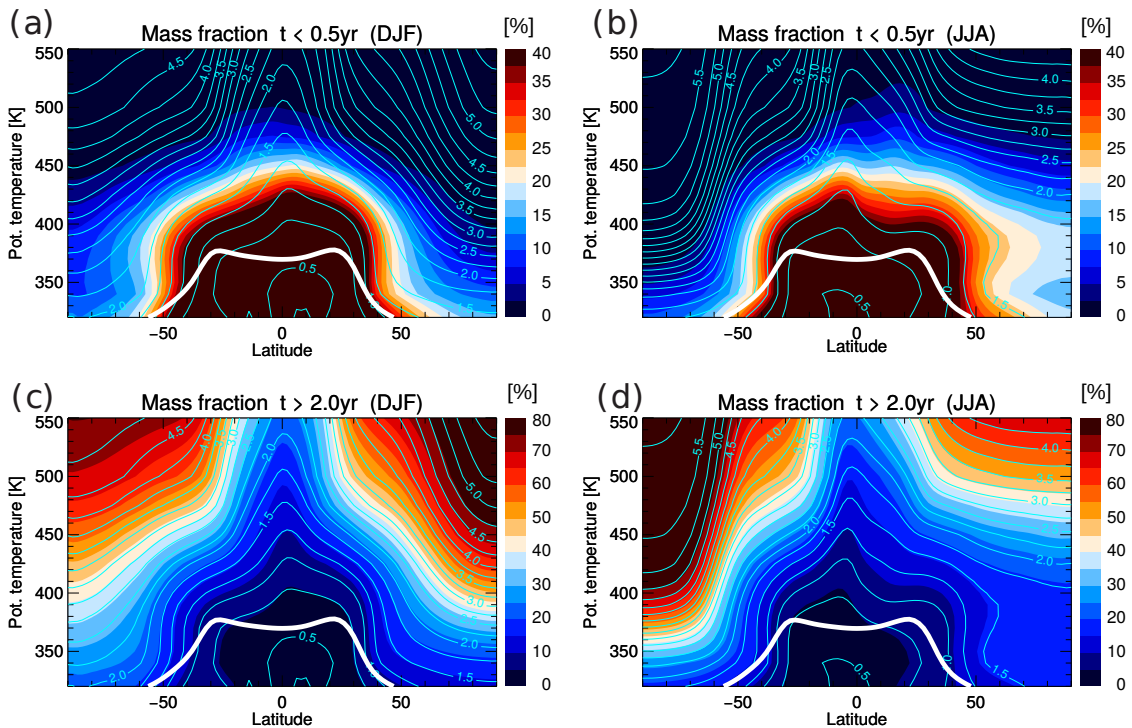


Figure 7. Fresh air fraction F_6 (transit time below 6 months) during (a) December–February, and (b) June–August. (c) and (d) show the fraction of old air (transit time above 2 years). The white contour shows the thermal tropopause, cyan contours show mean age.

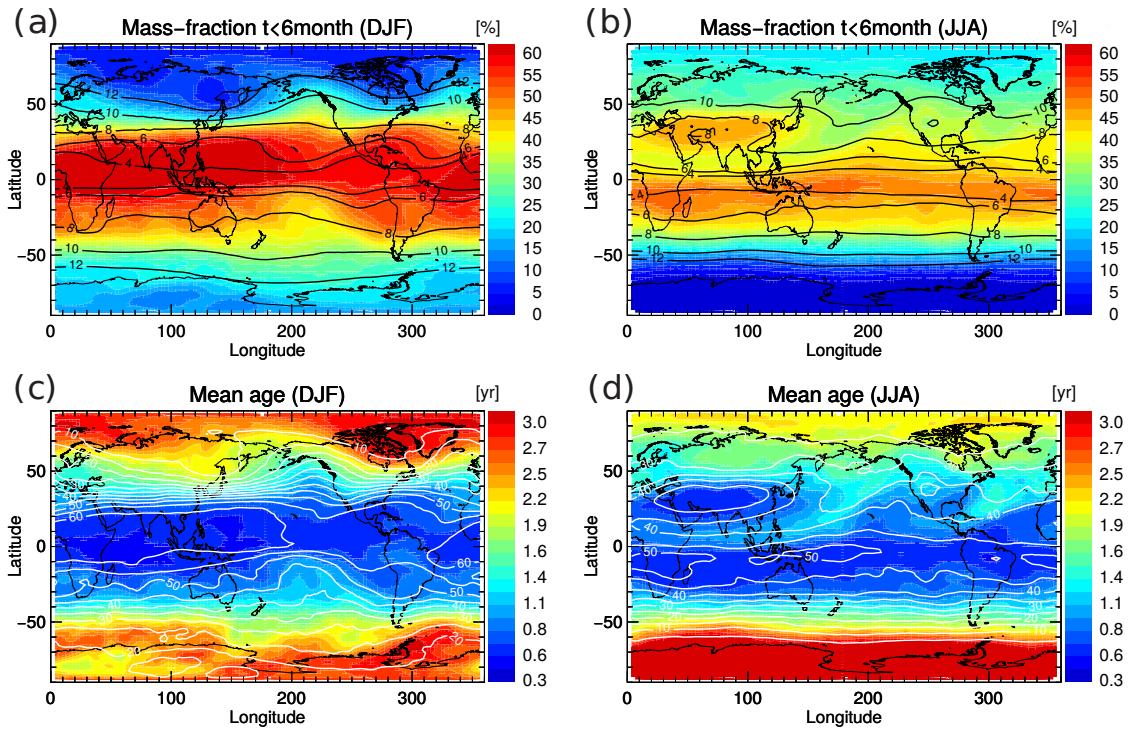


Figure 8. Fresh air fraction F_6 (transit time below 6 months) at 400 K during (a) December–February, and (b) June–August. Black contours show potential vorticity from ERA-Interim ($\pm 4, \pm 6, \pm 8, \pm 10, \pm 12$ PVU). (c) Mean age at 400 K during December–February, and (d) June–August (white contours illustrate the fresh air fractions from a/b).

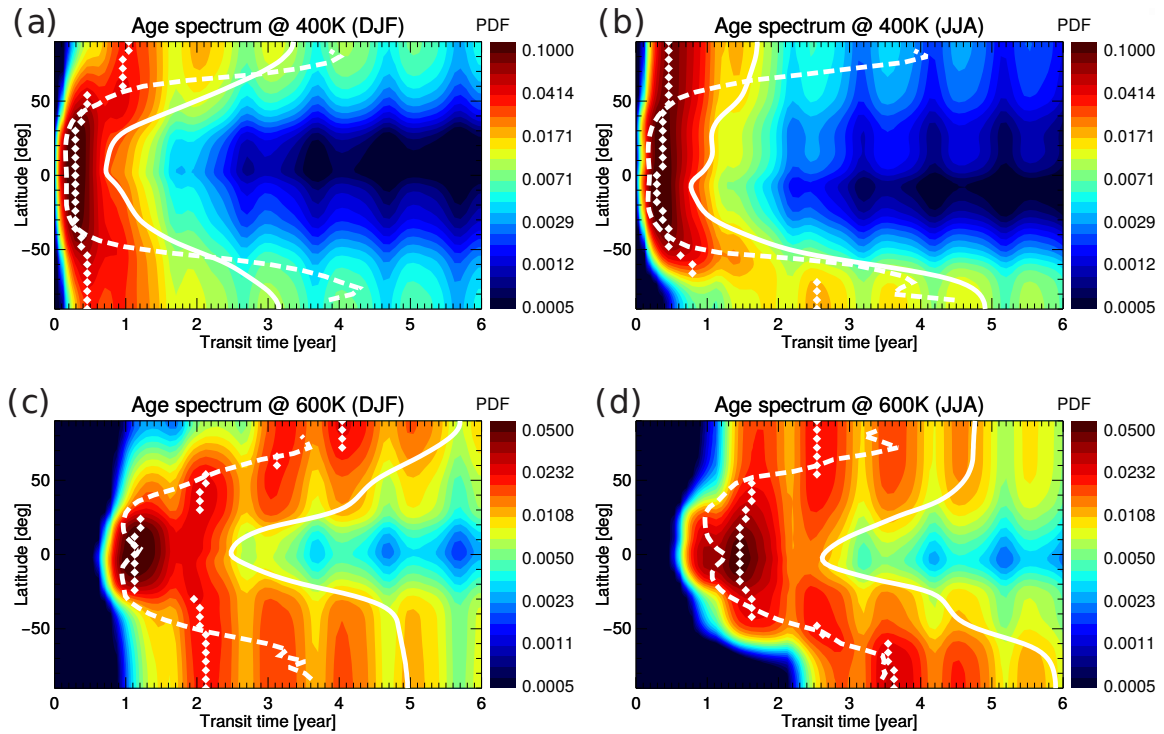


Figure 9. Age spectra at 400 K for (a) December–February and (b) June–August. (c) and (d) show the same but at 600 K. White lines show mean age (solid) and the residual circulation transit time (dashed). White diamonds show modal age.

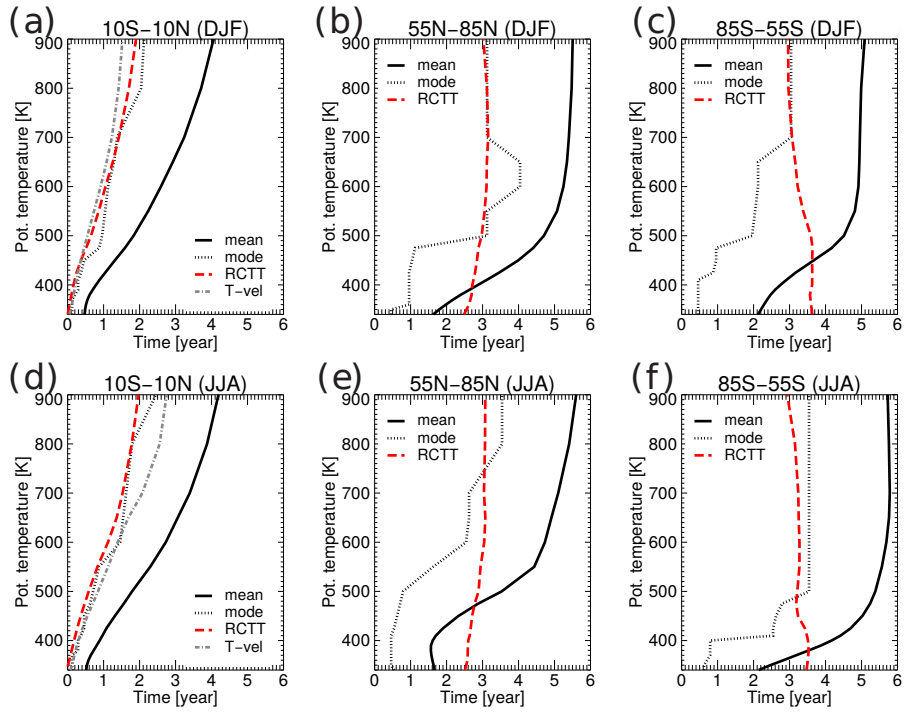


Figure 10. Profiles of mean age, modal age and RCTT for DJF (top) and JJA (bottom) at the equator, in the NH between 55°N – 85°N , and in the SH between 55°S – 85°S (from left to right). The grey dashed line in (a) and (d) shows the mean tropical upwelling time scale estimated from the zonal mean vertical velocity.

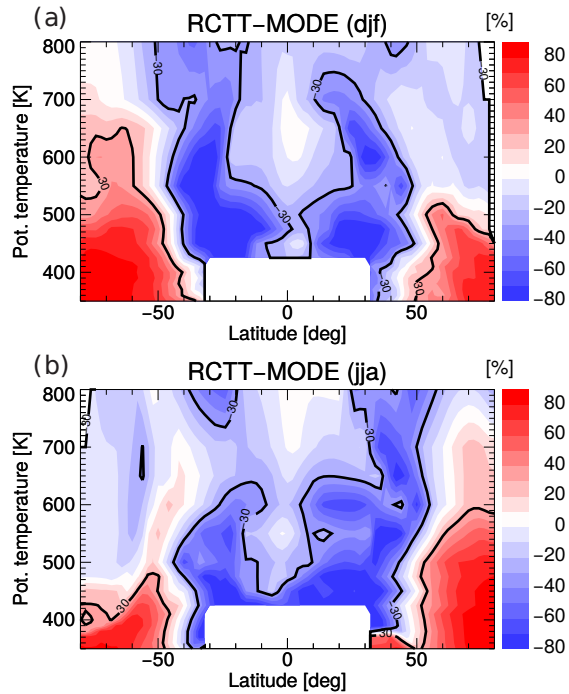


Figure 11. Difference between RCTT and modal age $(\text{RCTT} - \text{mode})/\text{RCTT}$ in percent for (a) December–February, and (b) June–August. The black line highlights the 30% contour. The tropical lowest stratosphere (below 420 K) is left white as relative differences become arbitrarily large there due to small transit times.

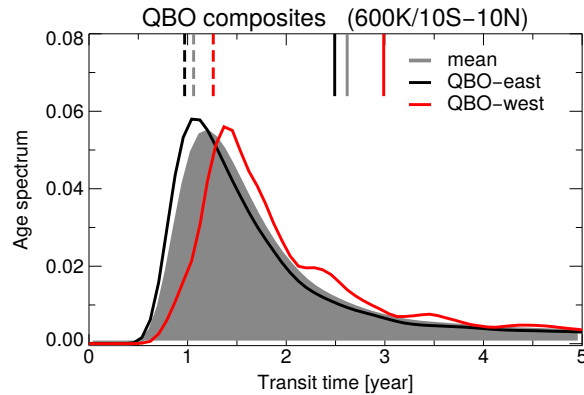


Figure 12. Age spectrum composites for easterly (black) and westerly (red) QBO phases, calculated from tropical (10°S – 10°N) CLaMS age spectra at 600 K. Mean ages are shown as solid vertical lines, RCTTs as dashed lines. The climatological mean spectrum, mean age and RCTT are shown in grey. (For better clarity of the differences, the westerly/easterly composites have been defined using the condition that ERA-Interim tropical mean zonal winds at 600 K go above/below $\pm 10\text{m/s}$).

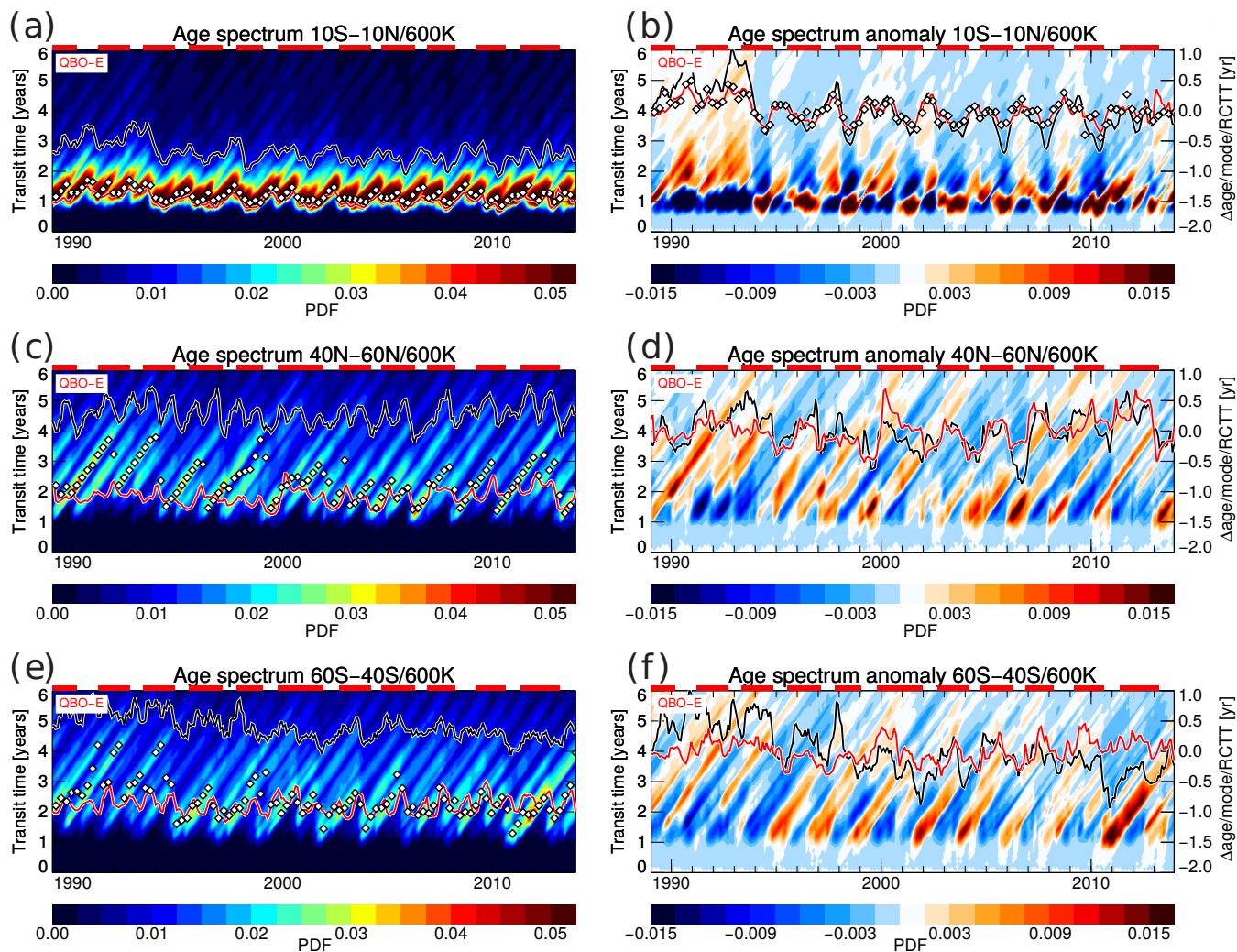


Figure 13. Age spectrum time series at 600 K and 10°S–10°N (top), 40°N–60°N (middle), and 60°S–40°S (bottom). Shown are the spectra (left) and their deseasonalized anomalies (right). Black lines show mean age, symbols modal age, and red lines show RCTT (full values on the left and their respective deseasonalized anomalies on the right). Red horizontal bars highlight easterly QBO phases.

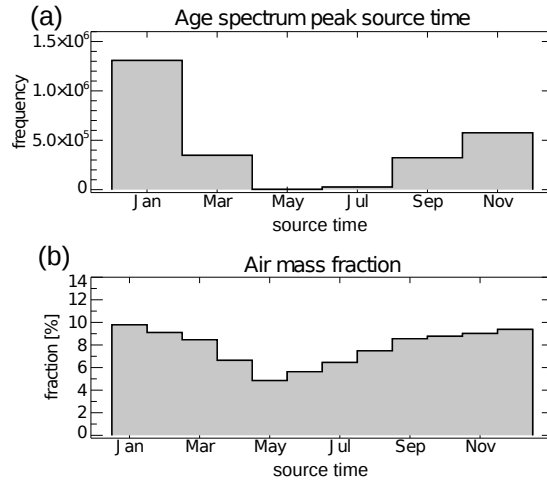


Figure 14. (a) Distribution of time of last contact with the boundary surface (source time) for age spectrum peak air. (b) Seasonality of time of last contact with the boundary surface for all stratospheric air masses. The distributions have been calculated from all CLaMS age spectra in the 380–1000 K potential temperature layer during the 1989–2013 period.

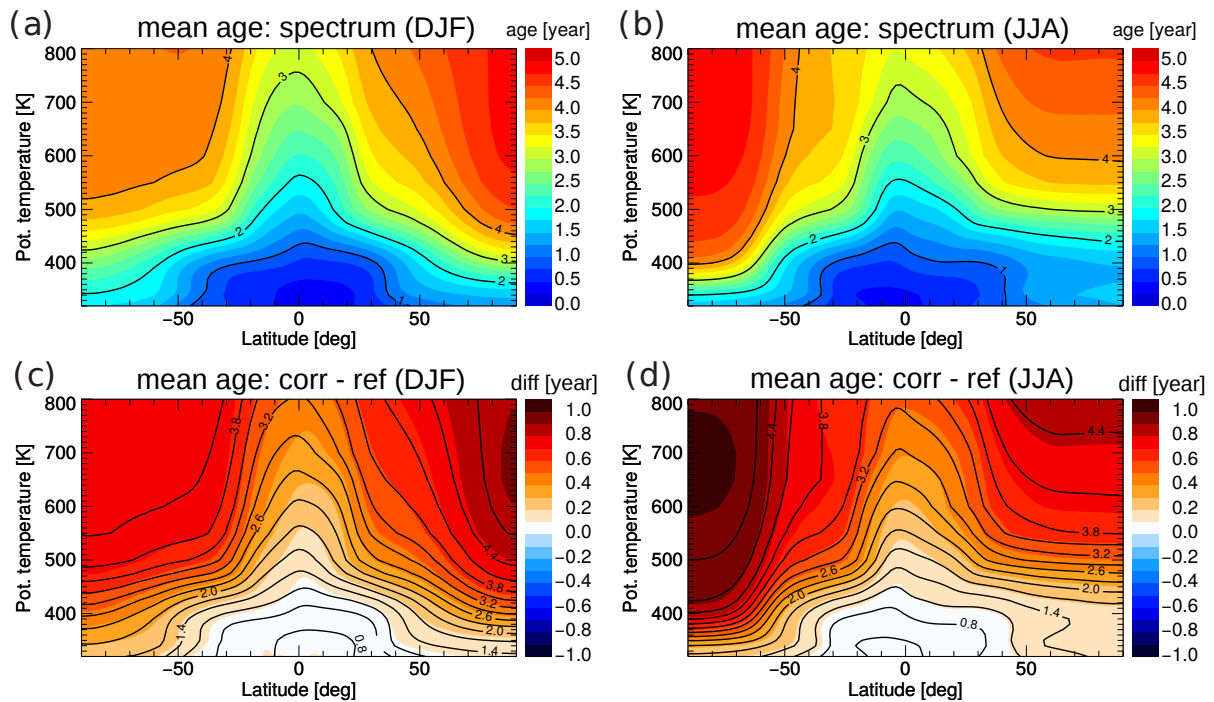


Figure 15. Climatological mean age from CLaMS age spectrum for (a) December–February and (b) June–August, without applying the tail-correction (see text). (c) and (d) show the difference of age spectrum mean ages with correcting for the finite spectrum tail to this reference. Black lines highlight particular mean age contours.